Robotica (2015) volume 33, pp. 884–897. © Cambridge University Press 2014
doi:10.1017/S0263574714000666

Dynamic rolling analysis of triangular-bipyramid robot

Yaobin Tian and Yan-An Yao*

School of Mechanical, Electronic and Control Engineering, Beijing Jiaotong University, Beijing 100044, P. R. China

(Accepted February 17, 2014. First published online: March 19, 2014)

SUMMARY

In this paper a rolling robot resembling the shape of a triangular-bipyramid is proposed. The robot has three degrees of freedom and is formed by connecting two tripod mechanisms with three spherical joints. By kinematic analysis, the robot can be viewed as a planar four-bar linkage. Further, its dynamic rolling ability is discussed by *Zero Moment Point* (ZMP) analysis. We show that the robot has the capability to roll, adjust its step length, and switch rolling directions. These functions are verified by a series of simulations with a CAD (computer-aided design) model and experiments with a prototype.

KEYWORDS: Rolling robot; Parallel mechanism; Triangular-bipyramid; ZMP analysis.

1. Introduction

Rolling locomotion is an effective mobile mode on flat ground.[1] Plenty of methods and structures have been presented to realize rolling locomotion. Spherical robot is a classic rolling robot that rolls on the ground with its entire outer surface by controlling actuators inside.[2–8] The touching area of spherical robot is relatively small, so it can be easily controlled to realize rolling locomotion. However, it requires some sophisticated algorithms to change directions and it is fairly hard to keep stable.[9,10] To improve the locomotion capability of spherical robots, Keith *et al.*[11] used "Pneumatic Method" to design a novel deformable spherical rolling robot. Phipps and Minor[12] presented a "MorpHex" rolling robot that can deform into spherical robot or six-legged robot.

Some rolling robots realize the rolling function by deforming their geometry shapes. Sugiyama and Hirai[13] used soft materials to design a robot that can roll, crawl, and jump by deforming its body. Shibata and Hirai[14] further used Tensegrity structure[15] to design a kind of deformable structure for rolling. Sastra *et al.*[16] used several modular links to construct a closed-loop mechanism and realized the rolling function by deforming the shape of the loop. Also with modular units, some modular reconfigurable robots, each consisting of multiple loops, can roll by controlling the edge length of some loops.[17–20] A common characteristic of these robots is that their centroids as well as shapes are changing during the rolling course. However, a disadvantage of these robots is that the degree of freedom (DOF) of the robot is very large, and thus a loss of the rigidity of their bodies.

Recently, we have proposed a class of 4R rolling mechanisms with single DOF.[21] The rolling function is realized by changing its shape, but the rolling step length is fixed, and the rolling direction cannot be changed freely. To drive the mechanism to any position on the ground, we used an 8U parallel mechanism to construct a 2-DOF rolling mechanism.[22] Further, we presented a tetrahedron unit to enable the rolling function.[23]

In this paper, we put forward a rolling robot resembling the shape of a triangular-bipyramid. This can be viewed as an extension of the work in ref. [23]. We focus on the kinematic analysis and dynamic rolling analysis of the robot. We show that the robot can be deformed into a planar four-bar linkage, and the dynamic rolling ability is discussed using Zero Moment Point (ZMP) theory.

* Corresponding author. E-mail: yayao@center.njtu.edu.cn

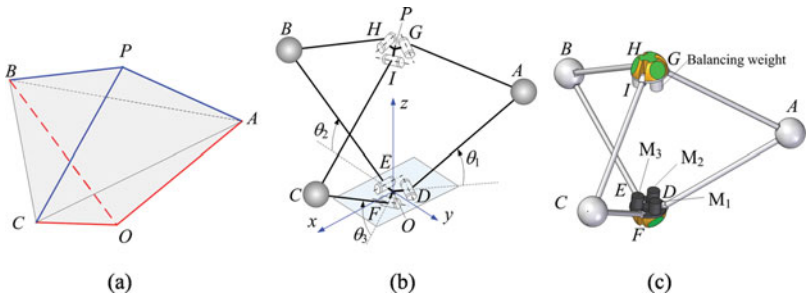

Fig. 1. The construction of a TBR: (a) the geometric of a triangular-bipyramid, (b) the sketch of TBR, (c) a three-dimensional (3D) model of the TBR.

The rest of the paper is organized as follows. The design of the robot is introduced in Section 2. Section 3 gives the kinematic analysis of the robot and shows that the robot can deform into a planar four-bar linkage. Section 4 discusses rolling capability based on ZMP analysis. Section 5 presents the results of the locomotion tests using a physical prototype. The conclusions and brief discussions close the paper in Section 6.

2. Mechanism Design

Figure 1 shows a triangular-bipyramid sketch with five vertexes and six triangles. It can be considered as two equal tripods (upper tripod *O-ABC* and lower tripod *P-ABC*) connected with their common face *ABC*. As shown in Fig. 1(b), each tripod mechanism contains a tripod link and three equal links, e.g., the lower tripod mechanism is composed of three links (*DA*, *EB*, and *FC*) and a tripod link *DEF* (see Fig. 1(b)). A *triangular-bipyramid robot* (for simplicity, called TBR) can be obtained by connecting two tripod mechanisms at vertexes *A*, *B*, and *C* with spherical joints. The three links are distributed around the tripod, and each link is connected to the tripod with a revolute joint. Therefore, the angle between every two axes of revolute joints is 60 deg. Point *O* and *P* are the center of the lower and upper platform respectively.

As shown in Fig. 1(b), the joints at *A*, *B*, and *C* are spherical joints. Therefore the TBR is a 3-RSR parallel mechanism, which contains eight links, six revolute joints, and three spherical joints. It is non-overconstrained (see, for example, in refs. [24] and [25]). Using Eq. (1) we get the mobility as

$$M = 6\,(n-1) - \sum_{i=1}^{g} (6 - f_i) = 6 \times 7 - 39 = 3. \tag{1}$$

See Fig. 1(c), three motors (M_1, M_2, and M_3) can be mounted at the lower platform to drive the links *DA*, *EB*, and *FC* respectively. A block is mounted at the upper platform to balance the weight of TBR.

3. Kinematic Analysis

In this section, we first do the position analysis of our robot. Based on the results, we show that the robot can be viewed as a four-bar linkage. Then, we further get the expression of some parameters of the four-bar linkage.

3.1. Position analysis

As shown in Fig. 1(a), initially, fix the lower platform of the mechanism on the ground; links *DA*, *EB*, and *FC* rotate about the lower platform for the angles of θ_1, θ_2 and θ_3 respectively. For the ease of discussion (seeing in Fig. 1(b)), a coordinate system *o-xyz* is set at the center of the lower platform (denoted as *O*). The *z*-axis is vertical to the ground, the *x*-axis is orthogonal to the link *BE*, and the *y*-axis is orthogonal to the plane of *xz*. Further, to simplify the analysis, we assume that the three revolute joints on the platform are very close to each other, and we can ignore the distance between the

https://doi.org/10.1017/S0263574714000666 Published online by Cambridge University Press

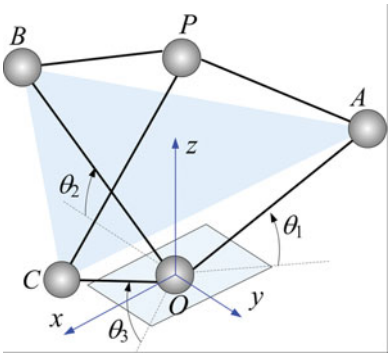

Fig. 2. The mathematic model of triangular-bipyramid robot.

revolute joints and the center of the platform. Figure 2 shows the simplified sketch of the mechanism, our goal is to get the expression of the positions of $\mathbf{r}_i$ $(i = A, B, C, P)$.

Recall that all the links have the same length. Let L be the length of line OA, let θ_1, θ_2, and θ_3 be the input angles of links OA, OB, and OC respectively. According to the mechanism, the positions of A, B, and C are determined by Eq. (2).

$$\begin{cases} \mathrm{r}_A = \left[-\frac{\sqrt{3}}{2} L\cos\theta_1 \quad \frac{1}{2} L\cos\theta_1 \quad L\sin\theta_1 \right]^T \\ \mathrm{r}_B = [0 \quad -L\cos\theta_2 \quad L\sin\theta_2]^T \\ \mathrm{r}_C = \left[\frac{\sqrt{3}}{2} L\cos\theta_3 \quad \frac{1}{2} L\cos\theta_3 \quad L\sin\theta_3 \right]^T \end{cases}. \tag{2}$$

Since $\|PA\| = \|OA\|$, $\|PB\| = \|OB\|$, and $\|PC\| = \|OC\|$, given the positions of A, B, and C, the position of P can be determined by Eq. (3).

$$\begin{cases} (r_{P,x} - r_{A,x})^2 + (r_{P,y} - r_{A,y})^2 + (r_{P,z} - r_{A,z})^2 = L^2 \\ (r_{P,x} - r_{B,x})^2 + (r_{P,y} - r_{B,y})^2 + (r_{P,z} - r_{B,z})^2 = L^2 \\ (r_{P,x} - r_{C,x})^2 + (r_{P,y} - r_{C,y})^2 + (r_{P,z} - r_{C,z})^2 = L^2 \end{cases} \tag{3}$$

For the three equations in Eq. (3), let the second and third equations minus the first one respectively, we have

$$\begin{cases} r_{P,x}(r_{B,x} - r_{A,x}) + r_{P,y}(r_{B,y} - r_{A,y}) + r_{P,z}(r_{B,z} - r_{A,z}) = 0 \\ r_{P,x}(r_{C,x} - r_{A,x}) + r_{P,y}(r_{C,y} - r_{A,y}) + r_{P,z}(r_{C,z} - r_{A,z}) = 0 \end{cases}. \tag{4}$$

Define $k_{11} = \frac{r_{B,y} - r_{A,y}}{r_{B,x} - r_{A,x}}$, $k_{12} = \frac{r_{B,z} - r_{A,z}}{r_{B,x} - r_{A,x}}$, $k_{21} = \frac{r_{C,y} - r_{A,y}}{r_{C,x} - r_{A,x}}$, and $k_{22} = \frac{r_{C,z} - r_{A,z}}{r_{C,x} - r_{A,x}}$, then Eq. (4) can be further simplified as

$$\begin{cases} r_{p,x} + k_{11} r_{P,y} + k_{12} r_{P,z} = 0 \\ r_{p,x} + k_{21} r_{P,y} + k_{22} r_{P,z} = 0 \end{cases}. \tag{5}$$

Define $a_1 = (-\frac{k_{11}(k_{22} - k_{12})}{k_{11} - k_{21}} - k_{12})$, $a_2 = \frac{k_{22} - k_{12}}{k_{11} - k_{21}}$, then solving Eq. (5), $r_{P,x}$ and $r_{P,y}$ can be expressed as

$$\begin{cases} r_{P,x} = a_1 r_{P,z} \\ r_{P,y} = a_2 r_{P,z} \end{cases}. \tag{6}$$

Substituting Eq. (6) into the first equation of Eq. (3), we have

$$(a_1 r_{P,z} - r_{A,x})^2 + (a_2 r_{P,z} - r_{A,y})^2 + (r_{P,z} - r_{A,z})^2 = L^2. \tag{7}$$

https://doi.org/10.1017/S0263574714000666 Published online by Cambridge University Press

Table I. Input angles $\{\theta_1, \theta_2, \theta_3\}$ (deg).

Input angles	θ_1	θ_2	θ_3
Congfig. a	30	60	36
Congfig. b	45	45	45
Congfig. c	0	60	0
Congfig. d	60	0	0
Congfig. e	0	0	60

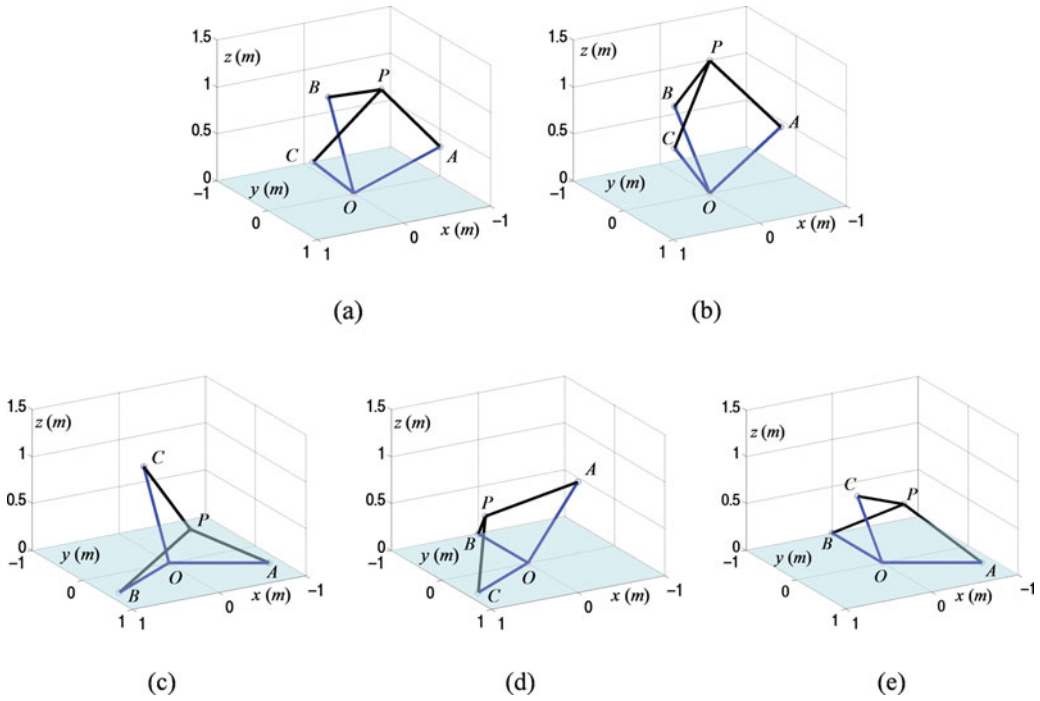

Fig. 3. The configurations (a)–(e) of the robot for kinematics with $\{\theta_1, \theta_2, \theta_3\}$ in Table I.

Using $r_{A,x}^2 + r_{A,y}^2 + r_{A,z}^2 = L^2$, Eq. (7) can be further simplified as

$$\left(a_1^2 + a_2^2 + 1\right) r_{P,z}^2 - 2(a_1 r_{A,x} + a_2 r_{A,y} + r_{A,z}) r_{P,z} = 0. \tag{8}$$

Since $r_{P,z}$ is non-negative, solving Eq. (8), we get

$$r_{P,z} = \frac{2(a_1 r_{A,x} + a_2 r_{A,y} + r_{A,z})}{a_1^2 + a_2^2 + 1}. \tag{9}$$

In the following we show a numerical example for the forward kinematics. From Eqs. (2), (6), and (9), all the vertices of the mechanism can be determined by the input angles θ_1, θ_2, and θ_3. Let $L = 1$. The parameters are shown in Table I. See Fig. 3, the configurations of the mechanism are obtained by running a program in Matlab.

Configuration (a) in Fig. 3 is an arbitrary state with three distinct θ_is; configuration (b) is a special state with $\theta_1 = \theta_2 = \theta_3$; configuration (c) is the case when $\theta_1 = \theta_3 = 0$ and $\theta_2 > 0$; configuration (d) is the case when $\theta_2 = \theta_3 = 0$ and $\theta_1 > 0$; configuration (e) is the case when $\theta_1 = \theta_2 = 0$ and $\theta_3 > 0$.

https://doi.org/10.1017/S0263574714000666 Published online by Cambridge University Press

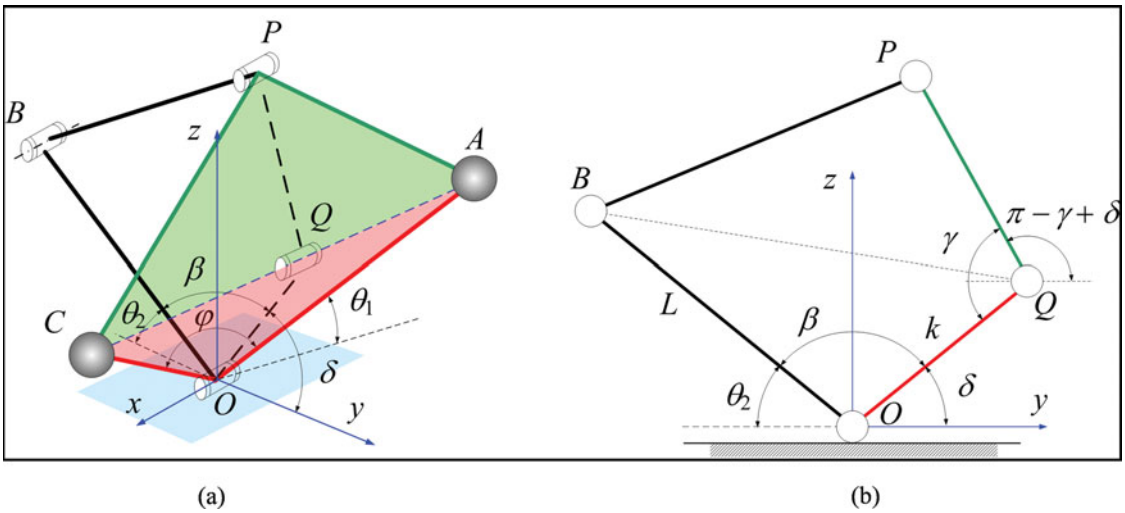

Fig. 4. The mathematic sketch of TBR: (a) the general state of the robot; (b) the projection view on the plane *OBP*.

3.2. Deform into a planar four-bar linkage

When two input angles are fixed and equal, for example (see Fig. 2), let $\theta_1 = \theta_3$, according to the kinematic analysis in Section 3.1, we have

$$\begin{cases} r_{A,x} = -r_{C,x}, r_{A,y} = r_{C,y}, r_{A,z} = r_{C,z} \\ r_{P,x} = r_{B,x} = 0 \end{cases}. \tag{10}$$

Since, $r_{P,x} = 0$, the upper platform can only move in the yz plane, and the mechanism is symmetrical with respect to the yz plane. As shown in Fig. 4(a), if we fix input angles θ_1 and θ_3, links OA and OC are fixed with the lower platform, such that, links OA, OC, and the lower platform can be considered as a single link OAC. By symmetry, links PA, PC, and upper platform become a single link PAC. Since links OAC and PAC are connected with two spherical joints, we can consider that links OAC and PAC are connected via a virtual revolute at point Q (the mid-point of AC). In this case, our mechanism can be viewed as a planar four-bar linkage. Figure 4(b) shows the projection view on the OBP plane. For convenience, the parameters of the four-bar linkage are defined as follows:

β, the angle between link OB and OQ;
γ, the angle between link OQ and QP;
φ, the angle between link OA and OC;
δ, the angle between link OQ and the positive y-axis;
k, the length of link OQ;
w, the length of line AC.

3.3. The parameters of the planar four-bar linkage

As shown in Fig. 4, a coordinate system is set at point O, the positive x-axis is vertical to the plane OBP, and the positive z-axis is vertical to the ground. When the input angle θ_1 is given, our goal is get the expression of parameters of β, γ, and k. As shown in Fig. 4(a), from triangle OAC, we have

$$k = L \cos \frac{\varphi}{2}. \tag{11}$$

Since φ is the angle of vector $\vec{OA}$ and $\vec{OC}$, using *vectorial angle cosine*, φ can be expressed as

$$\varphi = \arccos(1 - 1.5 \cos^2 \theta_1). \tag{12}$$

https://doi.org/10.1017/S0263574714000666 Published online by Cambridge University Press

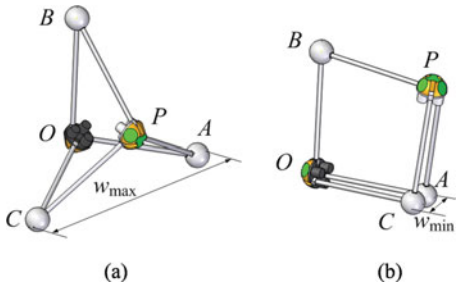

Fig. 5. The limit positions of line *AC*: (a) the maximum position; (b) the minimum position.

Using Eq. (12), we get the width as

$$w = 2L \sin \frac{\varphi}{2}. \tag{13}$$

When $\theta_1 = \theta_3 = 0$, line *AC* is at its maximum position (see Fig. 5(a)). When $\theta_1 = \theta_3 = 90^\circ$, line *AC* is at its minimum position (see in Fig. 5(b)), and the width of the robot is also very small at this position. Therefore, it is possible for the robot to roll across narrow passages.

In the planar four-bar linkage, if β is the input angle and γ can be considered as the output angle, then we can further express γ in terms of β. As shown in Fig. 4(b), let δ be the angle of link *OQ* and positive *y*-axis; then β can be written as

$$\beta = \pi - \delta - \theta_2, \tag{14}$$

where $\delta = \arctan(\frac{r_{Q,z}}{r_{Q,y}}) = \arctan(\frac{r_{A,z}+r_{C,z}}{r_{A,y}+r_{C,y}}) = \arctan(2\tan\theta_1)$.

Due to $\|OB\| = \|BP\| = L$, $\|DQ\| = \|QP\| = k$, according to *cosine theorem*, $\|BF\|$ can be determined as

$$\|BF\| = \sqrt{L^2 + k^2 - 2Lk\cos\beta} \tag{15}$$

By the *sine theorem* in triangle *OBQ*, angle γ satisfies

$$\sin\frac{\gamma}{2}/L = \sin\beta/\|BQ\|. \tag{16}$$

Combining Eqs. (15) and (16), we have

$$\gamma = 2\arcsin\left(\frac{L\sin\beta}{\sqrt{L^2 + k^2 - 2kL\cos\beta}}\right). \tag{17}$$

As shown in Fig. 6, when the robot is supported by point *O*, the height of the robot can be adjusted by changing the three input angles symmetrically. See Fig. 6(a), the upper platform of our robot is at its lowest position. In Fig. 6(c), the upper platform is at its highest position and the robot is also folding into a strut like structure. At this position, the robot can be easily stored and carried. When the robot rolls in the outdoor environment, this folding deformation is useful for hiding itself.

4. Dynamic Rolling Capability Analysis

In this section, the dynamic rolling function is analyzed based on ZMP of the mechanism. The ZMP is considered as the center of pressure at the feet (supporting area) on the ground.[26] Generally, ZMP is used to analyze the stability for walking robot. If the ZMP of a robot is in its interior of the supporting area, the robot is in a state of dynamic balance. Otherwise, if the ZMP moves out of the supporting area, the robot is about to lose the dynamic balance and rotate about its supporting

https://doi.org/10.1017/S0263574714000666 Published online by Cambridge University Press

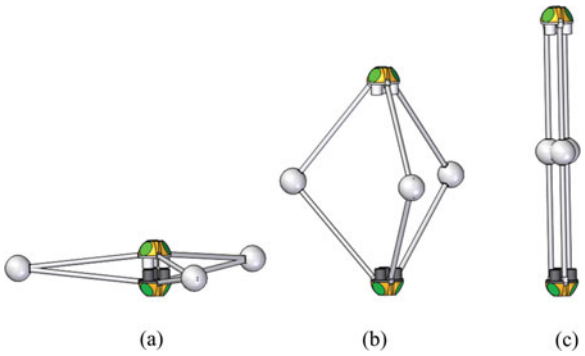

Fig. 6. The folding process: (a) the lower limit state; (b) the middle state; (c) the upper limit state.

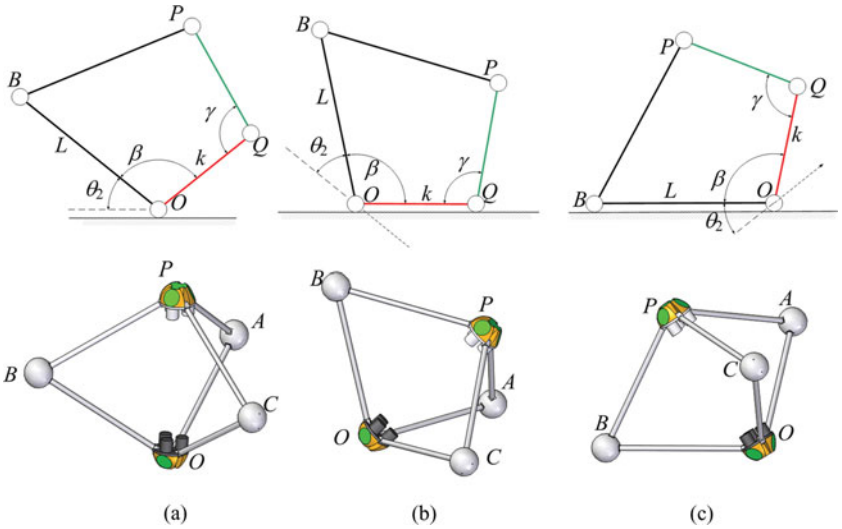

Fig. 7. The supporting states: (a) supporting by point O; (b) supporting by OB; (c) supporting by OA and OC.

edge. By controlling the ZMP out of the supporting links, our robot can realize the dynamic rolling locomotion.

4.1. ZMP analysis

As shown in Fig. 7, depending on the supporting state, we have three different cases, i.e., (a) supporting by O, (b) supporting by OA and OC, and (c) supporting by OB. The first line shows the corresponding four-bar linkage of the three supporting states, and the second line shows the 3D CAD (computer-aided design) models of the three supporting states.

For the first and third supporting states, we can control the centroid of the linkages out of its supporting point and the linkage will turn over onto the ground by its own gravity. So, in this section, we focus on discussing the ZMP of the second supporting state.

As shown in Fig. 8, recall that point Q is the position of the virtual revolute joint in Fig. 4, the four-bar linkage is supporting by OQ. A coordinate system is set at point O. The positive y-axis is along line OQ and the positive z-axis is vertical to the ground. Then it suffices to consider the component of the ZMP on the y-axis. We denote this component by y_{zmp}. According to the ZMP equations provided by Takanishi,[27] y_{zmp} can be expressed in Eq. (18).

$$y_{\text{zmp}} = \frac{\sum_{i=1}^{n} [m_i y_i (\ddot{z}_i + g_z) - m_i z_i \ddot{y}_i] + \left(\sum_{i=1}^{n} J_i \alpha_i\right)_x}{\sum_{i=1}^{n} m_i (\ddot{z}_i + g_z)}, \tag{18}$$

https://doi.org/10.1017/S0263574714000666 Published online by Cambridge University Press

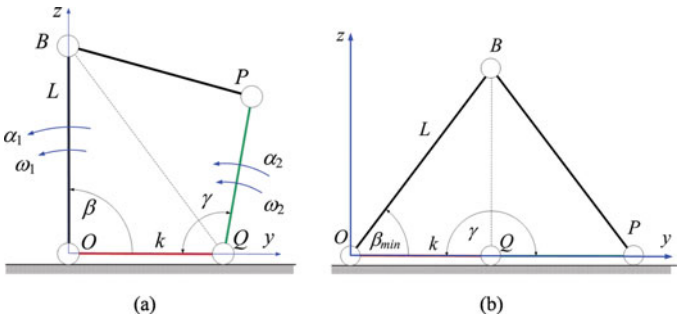

Fig. 8. The four-bar linkage *EBFD*: (a) the initial position, (b) the limit position of β.

where m_i is the mass of link i; $[y_i z_i]^T$ are the positions of the centroid of link i; $\ddot{x}_i$ and $\ddot{z}_i$ are the accelerations along the y-axis and z-axis respectively; g_z is the acceleration of gravity; and α_i is the angular acceleration of link i.

As shown in Fig. 8(a), for convenience, we use β and γ to express the positions of the four-bar linkage. Let ω_1 and α_1 be the angular velocity and acceleration of β respectively. Let ω_2 and α_2 be the angular velocity and acceleration of γ respectively. In the yoz plane, the position of O, B, P, and Q can be re-written as

$$[\,r_O \quad r_B \quad r_P \quad r_Q\,] = \begin{bmatrix} 0 & L\cos\beta & k(1-\cos\gamma) & k \\ 0 & L\sin\beta & k\sin\gamma & 0 \end{bmatrix}, \tag{19}$$

where γ is a function of β (see Eq. (17)).

Since the maximum value of γ is π, from Fig. 8(b), we can get the minimum value of β as

$$\beta_{\min} = \arccos\left(\frac{k}{L}\right). \tag{20}$$

Thus, the range of β is $(\beta_{\min}, p)$. From Eq. (19), we have

$$[\,\ddot{r}_O \quad \ddot{r}_B \quad \ddot{r}_P \quad \ddot{r}_Q\,] = \begin{bmatrix} 0 & u_1 & -u_2 & 0 \\ 0 & v_1 & v_2 & 0 \end{bmatrix}, \tag{21}$$

where

$$u_1 = L\big(-\alpha_1\sin\beta - \omega_1^2\cos\beta\big), \quad v_1 = L\big(\alpha_1\cos\beta - \omega_1^2\sin\beta\big),$$
$$u_2 = k\big(-\alpha_2\sin\gamma - \omega_2^2\cos\gamma\big), \quad v_2 = k\big(\alpha_2\cos\gamma - \omega_2^2\sin\gamma\big).$$

To determine the values of u_2 and v_2, ω_2 and α_2 should be solved further. According to Eq. (17), ω_2 can be obtained as

$$\omega_2 = \frac{\partial(\pi-\gamma)}{\partial t} = -\frac{2L\omega_1(L-k\cos\beta)(L\cos\beta-k)}{(L^2+k^2-2kL\cos\beta)\,|k-L\cos\beta|}. \tag{22}$$

Since $\beta \in (\arccos(k/L), \pi)$, we have $k - L\cos\beta \geq 0$, then Eq. (22) can be re-written as

$$\omega_2 = \omega_1\frac{2L^2-2kL\cos\beta}{L^2+k^2-2kL\cos\beta}. \tag{23}$$

Based on Eq. (23), we get

$$\alpha_2 = -\frac{2L\left(k\omega_1^2\sin\beta + L\alpha_1 - k\alpha_1\cos\beta\right)}{L^2+k^2-2kL\cos\beta} + \frac{4L^2\omega_1^2k(L-k\cos\beta)\sin\beta}{(L^2+k^2-2kL\cos\beta)^2}. \tag{24}$$

https://doi.org/10.1017/S0263574714000666 Published online by Cambridge University Press

Table II. The parameters of four-bar linkage when $\theta_1 = \theta_3 = 0$.

L (mm)	k (mm)	w (mm)	φ (deg)	$\beta_{\min}$ (deg)	m_1 (kg)	m_2 (kg)
250	125	433	120	60	2	0.5

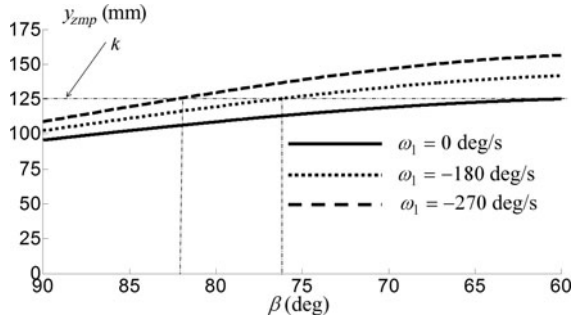

Fig. 9. The curves of y_{zmp} when $\omega_1 \leq 0$.

Since the motors are mounted on the platform and the links can be made of light materials, we only consider the mass of platforms (O and P) and the spherical joints (A, B, and C). Let lower and upper platforms have the same mass of m_1, and a spherical joint have a mass of m_2. So, the mass at points O, B, P, and Q are

$$\begin{bmatrix} m_O & m_B & m_P & m_Q \end{bmatrix} = \begin{bmatrix} m_1 & m_2 & m_1 & 2m_2 \end{bmatrix}. \tag{25}$$

Substituting Eqs. (19), (21) and (25) into Eq. (18), y_{zmp} is expressed as

$$y_{\text{zmp}} = \frac{m_1\left[u_2 k \sin\gamma - k\left(\cos\gamma - 1\right)\left(g + v_2\right) + \frac{k\alpha_2}{12}\right] + m_2\left[\left(g + v_1\right)L\cos\beta - u_1 L\sin\beta + 2gk + \frac{L\alpha_1}{12}\right]}{m_1\left(2g + v_2\right) + m_2\left(3g + v_1\right)}. \tag{26}$$

As shown in Fig. 8, when $y_{\text{zmp}} > k$, the mechanism will roll about point Q (the position of the virtual revolute joint in Fig. 4) along positive y-axis, and if $y_{\text{zmp}} < 0$, it rolls about point O along negative y-axis. Thus, the dynamic rolling condition is given in Eq. (27).

$$\begin{cases} y_{\text{zmp}} > k \\ y_{\text{zmp}} < 0 \end{cases}. \tag{27}$$

According to Eq. (26), when θ_1 and θ_3 are given, y_{zmp} is determined by the input parameters (i.e., ω_1 and α_1). Their relations are analyzed as follows:

Case 1: Link OB is rotating in the clockwise direction, with $\alpha_1 = 0$ and $\omega_1 \leq 0$.

Let $\theta_1 = \theta_3 = 0$, $L = 250$ mm. Based on the kinematic in Section 3, we get the parameters of four-bar linkage as shown in Table II. Suppose that the robot is moving from the initial position. Set $\omega_1 = 0, -180, -270$ deg/s, and β decreases from 90 deg to $\beta_{\min}$; the curves of y_{zmp} is plotted in Fig. 9.

When $\omega_1 = 0$, see the solid line in Fig. 9; y_{zmp} cannot move out of the upper limit. When $\omega_1 = -180$ deg/s, β is reducing from 90 deg to 60 deg. The relationship between y_{zmp} and β is shown in Fig. 9 (the dotted line). $\beta \approx 76.43$ deg, $y_{\text{zmp}} > k$, and the robot is beginning to roll about point Q.$\beta \in$ (76.43 deg, 90 deg), y_{zmp} is always in the interval of $[0, k]$, and the robot is kept stable. Further, when $\omega_1 = -270$ deg/s, the curve of y_{zmp} is shown through a dashed line. $\beta \approx 82.33$ deg, the $y_{\text{zmp}} > k$. We can see that the robot could roll to the right earlier as the value of ω_1 increases.

https://doi.org/10.1017/S0263574714000666 Published online by Cambridge University Press

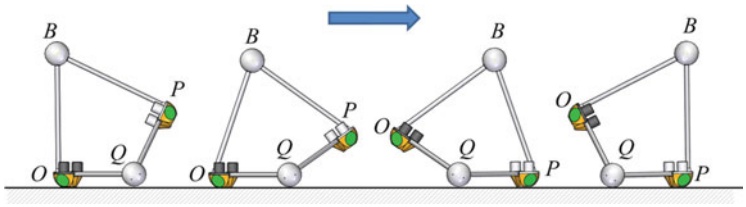

Fig. 10. The procedure of rolling to the right.

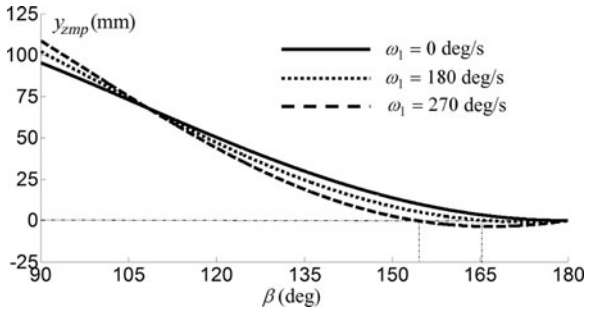

Fig. 11. The curves of y_{zmp} when $\omega_1 \geq 0$.

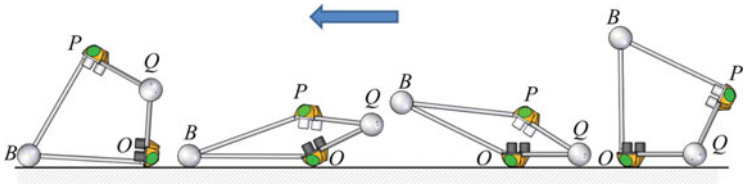

Fig. 12. The procedure of rolling to the left.

A rolling procedure of the mechanism is shown in Fig. 10. During this procedure, the rolling direction is fixed along line OQ, and the length of this rolling step is determined by $\|OQ\|$, i.e., k. When the rolling step is accomplished, the robot will have link PQ lying on the ground.

Case 2: Link OB is rotating in the counter-clockwise direction, with $\alpha_1 = 0$ and $\omega_1 \geq 0$.

Set $\omega_1 = 0, 180, 270$ deg/s. Consider that the robot is started at the initial state ($\beta = 90$ deg), so, β increases from 90 deg to 180 deg. The curves of y_{zmp} are plotted in Fig. 11. When $\omega_1 = 180$ deg/s, $\beta \approx 166.21$ deg, $y_{\text{zmp}} < 0$, and when $\omega_1 = 270$ deg/s, $\beta \approx 154.13$ deg, $y_{\text{zmp}} < 0$. Once $y_{\text{zmp}} < 0$, y_{zmp} is about to jump out of the lower limit and roll about point O along negative y-axis. Similarly with case 1, the robot can roll to the left earlier as the value of ω_1 increases.

A rolling procedure of the robot is shown in Fig. 12. After the rolling step, the robot will have link OB lying on the ground, resulting in the state that OB becomes the new supporting link.

Case 3: The angular acceleration $\alpha_1 \neq 0$.

In cases 1 and 2, we show that the angular velocity (ω_1) affects the curve of y_{zmp}. Further, in case 3, we discuss the effect of angular acceleration (α_1). For convenience, we suppose that our robot is moving to the right from the initial state with an initial angular velocity (κ) and a fixed angular acceleration (α_1). If the actuator is accelerated, e.g., $\kappa = -180$deg/s, $\alpha_1 = -57.3, -114.6$ deg/s^2, Fig. 13 plots the curves of y_{zmp} when the robot rolls to the right side. See Fig. 13, the ZMP is changed faster, and the robot will roll earlier as the value of $|\alpha_1|$ increases. If the actuator is decelerated, the robot will roll later as the value of α_1 increases.

By controlling the ZMP, the robot will roll along a straight line with four links supporting on the ground in turn.

https://doi.org/10.1017/S0263574714000666 Published online by Cambridge University Press

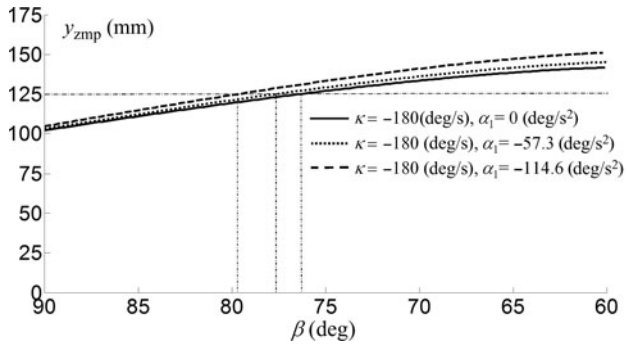

Fig. 13. The curves of y_{zmp} when $\omega_0 = -180$ deg/s, $\alpha_1 \leq 0$.

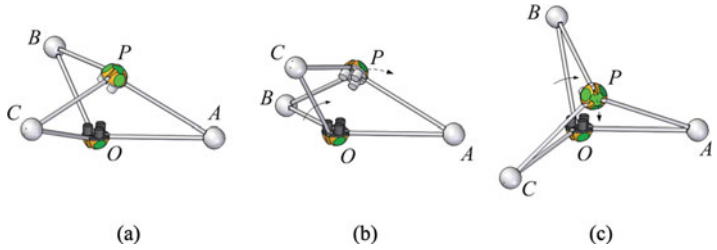

Fig. 14. Direction switching: (a) the state of the robot with *OA* lying on the ground; (b) the state of the robot with *OA* and *OB* lying on the ground; (c) the state of the robot with *OA* and *OC* lying on the ground.

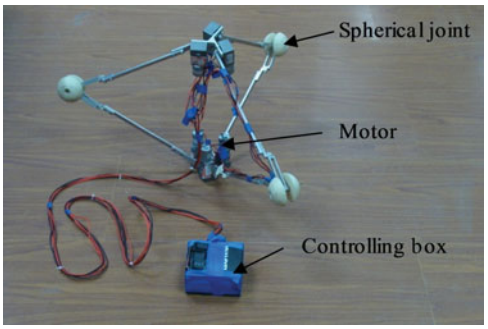

Fig. 15. The manufactured prototype.

4.2. Direction switching

When the robot is supported by single link, e.g., supported by link *OA* (see Fig. 14(a)), it is symmetrical with respect to line *OA*, and the projection of the centroid of the robot is within line *OA*. If link *OC* is rotated to increase the height of *C*, then point *P* will move along the dashed line (see Fig. 14(b)). Thereafter, the projection of the centroid of the robot will move out of line *OA* and the robot will roll about link *OA* toward *B*. As a result, see Fig. 14(b), *OA* and *OB* both lie on the ground. Alternatively, if link *OB* is rotated to increase the height of *B*, *OA* and *OC* both lie on the ground (see Fig. 14(c)). Therefore, the robot can change its rolling directions with a link supporting on the ground.

5. Prototype and Experiments

To test the feasibility and efficiency of the rolling robot in practice, a prototype is manufactured (Fig. 15). The parameters of the prototype are shown in Table III. Based on the prototype, Fig. 16 shows the folding function of our robot. Figure 17 shows that the robot changes its width. Figure18 shows a rolling experiment when the robot is at its narrowest state. As shown in Fig. 19, a rolling experiment is performed and the robot is rolling along a straight line. Figures 20 and 21 show the procedure of altering the rolling directions.

https://doi.org/10.1017/S0263574714000666 Published online by Cambridge University Press

Table III. Specification of the robot.

Item	Specification
Total weight	4.8 kg
Length of each link	250 mm
DC motor	12 V, speed: 0–360 deg/s, weight: 0.50 kg
Radius of spherical joint	50 mm
Rolling speed	Highest speed: 125 mm/s Lowest speed: 60 mm/s

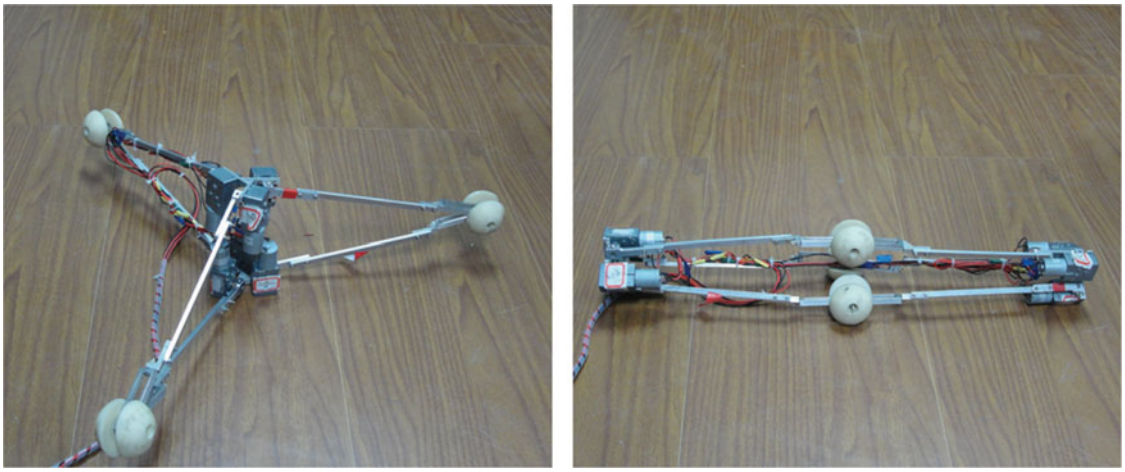

Fig. 16. The folding function.

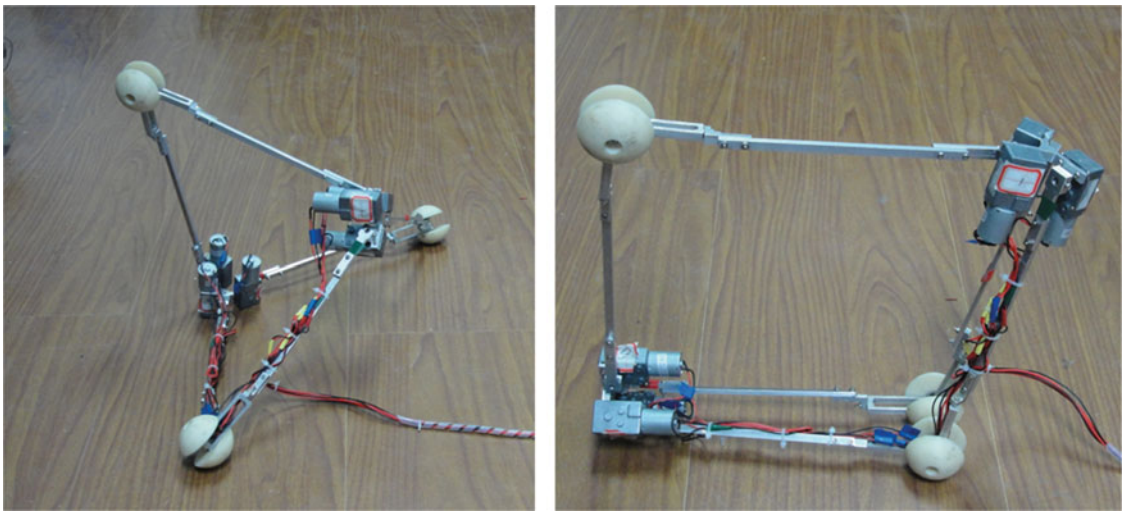

Fig. 17. The width adjustment.

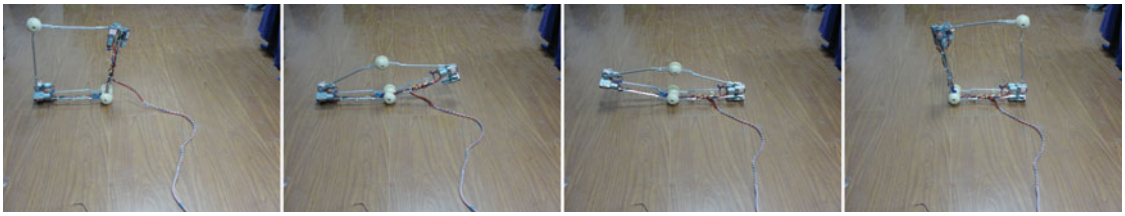

Fig. 18. A rolling procedure when the robot is at its narrowest state.

https://doi.org/10.1017/S0263574714000666 Published online by Cambridge University Press

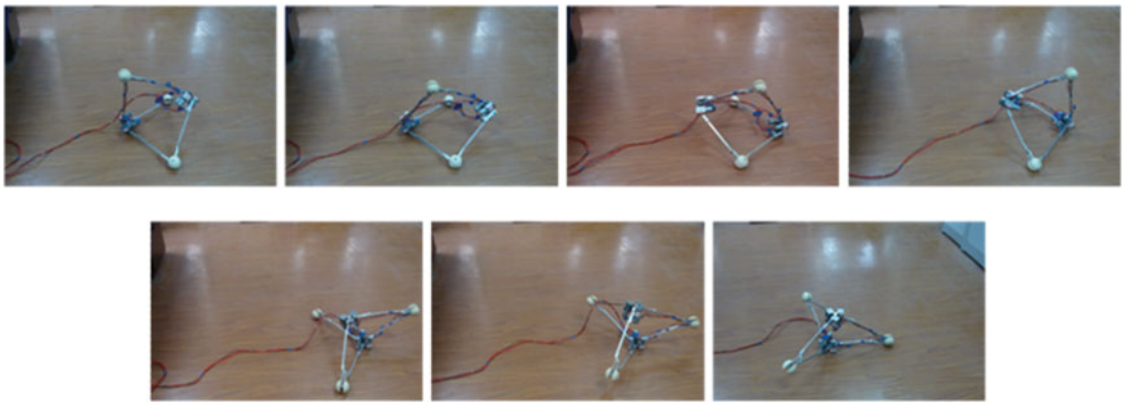

Fig. 19. Rolling along a straight line.

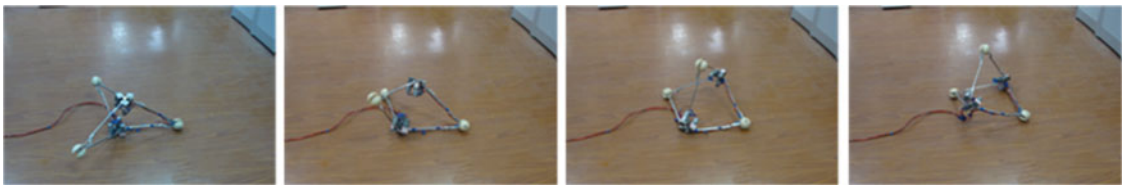

Fig. 20. A procedure of altering the rolling direction (rolling to one side of the robot).

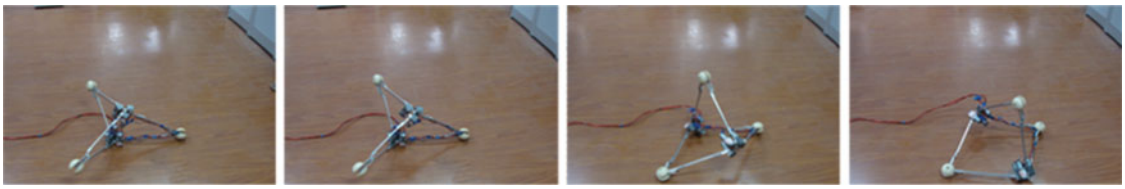

Fig. 21. A procedure of altering the rolling direction (rolling to other side of the robot).

6. Conclusions

In this paper, a rolling robot is proposed. It is essentially a combination of two tripod mechanisms into the geometry shape of a triangular bipyramid. Each tripod mechanism is realized by connecting three equal links at a common node via three revolute joints. The two tripod mechanisms are connected at their three common vertices via sphere joints. As regards to parallel robot, our robot is a 3-RSR parallel mechanism with 3 DOF. Based on the kinematic analysis, the deformation characteristics of the robot are revealed. With these characteristics, we show that our robot can be deformed into a planar four-bar linkage. The dynamic rolling capability is discussed by ZMP analysis of the planar four-bar linkage. We show that the robot can roll and change its rolling directions with proper conditions.

In addition, our robot can change the length of its rolling step and the width of the body during the rolling process. With this feature, the robot is capable to rolling across narrow passages. Further, we show that the robot can be folded into a strut-like structure, which can be very useful in carrying and storing or exploring the unstructured environments. Finally, a series of experiments were performed on a real prototype of the robot. In the future, we would like to extend the work in two directions. First, we would like to optimize the parameters of the designs to improve the rolling performance. Second, we would like to study the path planning on rugged surfaces.

Acknowledgements

This work was supported by National Natural Science Foundation of China (51175030), Fundamental Research Funds for the Central Universities (2012JBZ002), and a project supported by Chinese Ministry of Education (625010403).

https://doi.org/10.1017/S0263574714000666 Published online by Cambridge University Press

References

1. T. Ylikorpi and J. Suomela, "Ball shaped robots: An historical overview and recent development at TKK," *Field Serv. Rob.* **25**(6), 343–354 (2006).
2. R. H. Armour and J. F. Vincent, "Rolling in nature and robotics: A review," *J. Bionic. Eng*. **3**(4), 195–208 (2006).
3. A. Halme, T. Schönberg and Y. Wang, "Motion Control of a Spherical Mobile Robot," *Proceedings of IEEE International Workshop on Advanced Motion Control*, Mie, Japan (May. 18–21, 1996) pp. 259–264.
4. A. Bicchi, A. Balluchi, D. Prattichizzo and A. Gorelli, "Introducing the Sphericle: An Experimental Testbed for Research and Teaching in Non-Holonomy," *Proceedings of IEEE International Conference on Robotics and Automation*, Albuquerque, USA (Apr. 20–25, 1997) pp. 2620–2625.
5. T. Otani, T. Urakuboi, S. Maekawa, H. Tamaki and Y. Tada, "Position and Attitude Control of a Spherical Rolling Robot Equipped with a Gyro," *9th IEEE International Workshop on Advanced Motion Control*, Istanbul, Turkey (Mar. 27–29, 2006) pp. 416–421.
6. R. Mukherjee, M. A. Minor and J. T. Pukrushpan, "Simple Motion Planning Strategies for Spherobot: A Spherical Mobile Robot," *Proceedings of IEEE International Conference on Decision and Control*, Phoenix, USA (Dec. 7–10, 1999) pp. 2132–2137.
7. R. Mukherjee, M. A. Minor and J. T. Pukrushpan, "Motion planning for a spherical mobile robot: Revisiting the classical ball-plate problem," *ASME J. Dyn. Syst.-T.* **124**, 502–511 (2002).
8. A. H. Javadi and P. Mojabi, "Introducing glory: A novel strategy for an omnidirectional spherical rolling robot," *ASME J. Dyn. Syst.-T.* **126**(3), 678–683 (2004).
9. V. A. Joshi and R. N. Banavar, "Motion analysis of a spherical mobile robot," *Robotica* **27**, 343–353 (2009).
10. V. A. Joshi, R. N. Banavar and R. Hippalgaonkar, "Design and analysis of a spherical mobile robot," *Mech. Mach. Theory* **45**, 130–136 (2010).
11. K. W. Wait, P. J. Jackson and L. S. Smoot, "Self Locomotion of a Spherical Rolling Robot Using a Novel Deformable Pneumatic Method," *IEEE International Conference on Robotics and Automation*, Anchorage, USA (May. 3–8, 2010) pp. 3757–3762.
12. C. C. Phipps and M. A. Minor, "Introducing the hex-a-ball, a hybrid locomotion terrain adaptive walking and rolling robot," *Proceedings of Climbing and Walking Robots (CLAWAR)*, London, UK (Sept. 13–15, 2005) pp. 525–532.
13. Y. Sugiyama and S. Hiral, "Crawling and jumping by a deform robot," *Int. J. Robot. Res.* **25**(5–6), 603–620 (2006).
14. M. Shibata and S. Hiral, "Rolling Locomotion of Deformable Tensegrity Structure," *12th International Conference on Climbing and Walking Robots and the Support Technologies for Mobile Machines*, Istanbul, Turkey (Sep. 9–11, 2009) pp. 1–8.
15. C. R. Calladine, "Buckminster fuller's "Tensegrity" structures and Clerk Maxwell's rules for the construction of stiff frames," *Int. J. Solids Struct.* **14**, 161–172 (1978).
16. J. Sastra, S. Chitta and M. Yim, "Dynamic rolling for a modular loop robot," *Int. J. Robot. Res.* **28**(6), 758–773 (2009).
17. M. Yim, D. G. Duff and K. D. Roufas, "PolyBot: A Modular Reconfigurable Robot," *Proceeding of the 2000 IEEE International Conference on Robotics and Automation*, San Francisco, USA (Apr. 24–28, 2000) pp. 514–520.
18. W. H. Lee and A. C. Sanderson, "Dynamic rolling locomotion and control of modular robots," *IEEE T. Robotic. Autom.* **18**(1), 32–41 (2002).
19. P. E. Clark, M. L. Rilee, S. A. Curtis, W. Truszkowski, G. Marr, C. Cheung and M. Rudisill, "BEES for ANTS: Space Mission Applications for the Autonomous Nanotechnology Swarm," *Proceedings of the 1st AIAA Intelligent Systems Technical Conference*, Chicago, USA (Sep. 20–22, 2004), Session 29-IS-13, pp. 1–12.
20. A. Lyder, R., Franco, M. Garcia and K. Stoy, "Mechanism Design of Odin, an Extendable Heterogeneous Deformable Modular Robot," *Proceeding of the 2008 IEEE/RSJ International Conference on Intelligent Robots and Systems*, Nice, France (Sept. 22–26, 2008) pp. 883–888.
21. C. H. Liu, Y. A. Yao, R. M. Li, Y. B. Tian, N. Zhang, Y. Y. Ji and F. Z. Kong, "Rolling 4R linkages," *Mech. Mach. Theory* **48**, 1–14 (2012).
22. C. H. Liu, R. M. Li and Y. A. Yao, "An omnidirectional rolling 8U parallel mechanism," *ASME J. Mech. Robot.* **4**(3), 034501-1–034501-06 (2012).
23. Y. B. Tian and Y. A. Yao, "Constructing Rolling Mechanisms Based on Tetrahedron Units," *Proceedings of the International Conference on Reconfigurable Mechanisms and Robots (ReMAR 2012)*, Tianjin, China (Jul. 9–11, 2012) pp. 221–232.
24. D. R. Dunlop and T. P. Jones, "Position analysis of a 3-DOF parallel manipulator," *Mech. Mach. Theory* **32**(8), 903–920 (1997).
25. M. Karouia and J. M. Hervé, "Asymmetrical 3-dof spherical parallel mechanisms," *Eur. J. Mech. A-Solid* **24**(1), 47–57 (2007).
26. M. Vukobratović, A. A. Frank and D. Juricic, "On the stability of biped locomotion," *IEEE T. Bio-Med. Eng.* **17**(1), 25–36 (1970).
27. A. Takanishi, M. Tochizawa, T. Takeya, H. Karaki and I. Kato, "Realization of Dynamic Biped Walking Stabilized with Trunk Motion Under Known External Force," *Proceedings of the 4th International Conference on Advanced Robotics*, Columbus, USA (Jun. 13–15, 1989) pp. 299–310.